Available online at www.sciencedirect.com
SCIENCE DIRECT®
ELSEVIER
European Journal of Mechanics B/Fluids 22 (2003) 317–329
EUROPEAN JOURNAL OF MECHANICS B/FLUIDS

Two-dimensional perturbations in a suddenly blocked channel flow

Pietro Scandura

Department of Civil and Environmental Engineering, University of Catania, Viale Andrea Doria, 6, 95125 Catania, Italy

Received 13 August 2002; received in revised form 12 February 2003; accepted 13 August 2003

Abstract

The stability of the laminar flow established after the sudden closure of a channel is investigated by numerical simulations of the Navier–Stokes and continuity equations. The basic flow computed by the present approach agrees satisfactorily with the one obtained by other authors using a Pohlhausen technique. A stability analysis performed computing the time development of 2-D perturbations of small amplitude shows that the flow is more unstable than predicted by a quasi-steady approach. The large amplitude perturbations detected in previous experimental visualizations of decelerating channel and pipe flows are qualitatively reproduced. The results of the simulations show that the amplification of the perturbation is accompanied by the formation of vortices which survive for long time. Finally, the spatial longitudinal energy spectrum is examined and the existence of a wavenumber range in which the slope of the spectrum ranges from -3 to -4 is observed. The numerical simulations in the nonlinear regime allow to have a deeper insight into the physical mechanism leading to the appearance of turbulence.

Keywords: Flow blockage; Stability; Vorticity

1. Introduction

The flow which follows the sudden blockage of a laminar channel flow, such that produced by the rapid closure of a valve, is of practical relevance. Indeed, sudden blockage of flows arises in a variety of devices and applications ranging from physiological flows to water pipes. The sudden closure of a channel imposes new boundary conditions which force a rapid deceleration of the flow.

Experimental observations under different unsteady flows have shown that when a flow decelerates, small disturbances can grow and lead to the appearance of turbulence. In particular, in the Stokes boundary layer disturbances grow explosively at the start of the decelerating phase of the cycle [1,2], as also shown in physiological flows where high frequency disturbances have been detected during the decelerating phase of the flow in the aorta [3]. In order to explain the origin of turbulence observed in the latter case, Weinbaum and Parker [4] performed some experimental visualizations in a decelerating pipe flow. In these experiments the behaviour of dye streaks and hydrogen bubbles after the sudden closure of a valve at the downstream end of a horizontal straight pipe was observed. When the Reynolds number, based on diameter and mean velocity before the valve is closed, was less than approximately 2000 a stable laminar decay was observed. For higher Reynolds numbers a periodic streamwise instability, which eventually leads to turbulence, was detected. More recently, Das and Arakeri [5] have performed a series of experimental visualizations of the instability that takes place in a decelerating flow both in a pipe and in a channel. The flow was generated by a piston which traveled for a certain distance at constant velocity before starting to decelerate. The instability was detected during the decelerating phase. In these experiments viscous effects did not have enough time to propagate up to the channel centerline, then an irrotational core region was present before the start of the decelerating phase. For some values of the parameters that characterize the flow, Das and Arakeri [5] observed large amplitude perturbations which

E-mail address: pscandu@dica.unict.it (P. Scandura).

0997-7546/$ – see front matter
doi:10.1016/S0997-7546(03)00037-2

seem in very good agreement with the descriptions reported by Weinbaum and Parker [4], even though in the latter case the basic flow was characterized by a fully developed Poiseuille velocity profile.

The flow observed in the above mentioned experiments is similar to that determined in pipes when a valve is suddenly closed (water hammer phenomenon), which is a case of interest in hydraulic engineering. Indeed, the development of mathematical models of water hammer has been pursued by the hydraulic engineering community for many years. Comparison of the model predictions with the experimental data shows a good agreement for practical purposes, both for laminar and turbulent flows. However, room for improvement exists as some discrepancies between model predictions and experimental data are still present [6]. The models which have been proposed up to now do not take into account the instability phenomenon described by Weinbaum and Parker [4] and Das and Arakeri [5] and this could be one of the possible explanations of their weakness.

The aim of the present paper is to investigate the aforementioned instability for the laminar channel flow to gain more insight into the structure of the flow field generated after the sudden stoppage.

Weinbaum and Parker [4] studied the laminar decay of the fully developed Poiseuille velocity profile in a channel that is suddenly closed. According to these authors, the flow develops on two time scales which vastly differ when it is observed in a region characterized by a longitudinal extent L of order of magnitude of the channel width h. The first time scale is the short one h/c_s. This time is characteristic of the propagation of the pressure wave induced by the valve closure, where c_s is the velocity of sound. The second is the larger time scale h^2/ν, which is characteristic of the viscous diffusion of momentum through the channel width, ν being the kinematic viscosity of the fluid. Introducing an appropriate scaling for the vorticity equation, Weinbaum and Parker [4] showed that, on the shorter time scale h/c_s, after the sudden stoppage, the vorticity $\underline{\omega}$ satisfies approximately the equation $\partial\underline{\omega}/\partial t = 0$ if $M \ll 1$ and $M/Re \ll 1$, where M is the Mach number and Re is the Reynolds number defined as $M = U_m/c_s$ and $Re = U_m h/\nu$, where U_m is the average velocity in the channel section prior to the sudden blockage of flow. The above mentioned conditions on the parameters M and M/Re are usually satisfied in flows of water. Under a physical point of view, this result is related to the fact that the pressure wave passes so quickly on the spatial scale of order h that the flow does not have enough time to change its vorticity appreciably. Thus, the passage of the pressure wave causes an irrotational velocity field to be superimposed on the former one. The solution of the inviscid velocity field is found by solving a Poisson equation [4].

It should be stressed that even though the fluid compressibility is neglected when solving the inviscid velocity field, it must be considered when the pressure rise that follows the sudden blockage must be computed.

Let us now consider the flow development in a region of longitudinal extent L that is not of the same order of magnitude as h and shortly analyze the conditions under which the assumption $\partial\underline{\omega}/\partial t \approx 0$ is still appropriate. If the rate of change of vorticity is negligible, we should have $h^2/\nu \gg L/c_s$ and $h/U_m \gg L/c_s$, where h/U_m is the convective timescale. By introducing the Mach number and the Reynolds number, these conditions can be rewritten as follows: $ML/(Reh) \ll 1$, $ML/h \ll 1$. These relations state respectively that diffusion and convection of vorticity are negligible during the time the pressure wave takes to cover the distance L. The second relation imposes more restrictions on the value of L because usually the Reynolds number is large. For example, if $h = 10^{-2}$ m and $M = 10^{-4}$, L should be less than 10 m in order that $ML/h < 10^{-1}$. In this example if L is much greater than 10 m, we need to resort the fluid compressibility in the governing equations.

The solution for the inviscid velocity field obtained by Weinbaum and Parker [4] shows that end effects are confined within a distance from the valve of the order of magnitude of the channel width and the flow remains elsewhere unidirectional. Moreover, beyond the above cited distance from the valve, the passage of the pressure wave gives rise to a uniform deceleration of the velocity profile by an amount equal to the average value of the initial Poiseuille velocity profile. Hence, the sudden closure of one end of the channel forces a zero net flow. The irrotational part of the velocity field does not satisfy the no-slip condition at the walls or, equivalently, it results in an infinitesimally thin vortex layer at the walls with infinite vorticity. Subsequently, this vorticity diffuses in the channel width and the flow tends to decay on the time scale h^2/ν. Since no further pressure waves can be generated during the diffusion process, the flow field can be studied by the incompressible Navier–Stokes equations. In particular, Weinbaum and Parker [4] obtained an approximate solution for the decaying velocity profile on the diffusive time scale using a Pohlhausen technique. Evidence of the correctness of the velocity profiles computed by the described approach can be gained by comparing the velocity profiles computed in [4] with that presented in the paper of Vardy and Hwang [7], who computed the flow taking into account the fluid compressibility.

Later, Hall and Parker [8] studied the linear stability of this flow analysing the first term of a Wentzel–Kramers–Brillouin expansion (WKB expansion) in powers of Re^{-1} of the stability equation. As shown in [8], the first term of the WKB expansion is equal to the disturbance equation obtained by a quasi-steady approach. Then, it was assumed that the growth of the instability occurs on a time scale over which the basic flow does not change significantly. Following this approach, the authors found instability at values of the Reynolds number of order 10^2, the instability being induced by the occurrence of an inflexion point in the decaying velocity profile. These theoretical findings explain the experimental observation of turbulence which takes place after flow blockage. However, since the theoretical analysis of Hall and Parker [8] considers small amplitude perturbations it cannot describe the development of the instability in the finite amplitude regime.

In this paper, the stability with respect to 2-D perturbations of the decaying velocity profile established after the sudden blockage is investigated numerically, by integrating the Navier–Stokes and continuity equations. The adopted approach allows both to remove the assumption of slowly varying basic flow [8] and to follow the development of perturbations in the nonlinear regime. The rest of the paper is organized as follows. In Section 2 the problem is formulated and the numerical method is briefly described. In Section 3 the results of a linear stability analysis are discussed and compared with the theoretical results of Hall and Parker [8]. Section 4 is devoted to the investigation of the perturbation development in the nonlinear regime. In the last section some conclusions are drawn.

2. Formulation of the problem

Let us consider a channel formed by two parallel plates of infinite extent within which a Poiseuille flow is established. A sketch of the problem is shown in Fig. 1. Hereinafter a star is used to denote dimensional quantities.

As in [4,8], we study the flow development in a region characterized by a longitudinal extent of the same order of magnitude as the channel width h^* and that is far enough away from the valve so that the basic flow after the sudden blockage can be considered unidirectional. This condition is satisfied at a distance from the valve larger than two times the channel width as shown by the results of [4]. In Fig. 1 we have also denoted the region of interest which extends from $x_1^* = 0$ to $x_1^* = L_{x_1}^*$. Note that the origin of the reference system does not coincide with the position of the valve.

The velocity components in the x_1^* and x_2^* directions are denoted by u_1^* and u_2^* respectively, the pressure by p^* and the time by t^*. In order to formulate the problem in dimensionless form, the following dimensionless variables are used,

$$(x_1, x_2) = \left(\frac{x_1^*, x_2^*}{h^*}\right), \quad (u_1, u_2) = \left(\frac{u_1^*, u_2^*}{U_m^*}\right), \quad t = \frac{t^* U_m^*}{h^*}, \quad p = \frac{p^*}{\varrho^* (U_m^*)^2}, \tag{1}$$

where U_m^* is the average value of u_1^* in the x_2^* direction and ϱ^* is the constant density of the fluid.

In the following the dimensionless time $t_d = 4\nu^* t^* / h^{*2}$ will also be used, where the factor 4 has been introduced to make t_d equal to the dimensionless time used in [8]. The relation between t and t_d is $t_d = 4t/Re$. In [8] it is shown that the most unstable velocity profile of the basic flow is established at a time t_d which is independent on the value of the Reynolds number. The time t_d is introduced to be used in the linear stability analysis presented in the following section, because it makes easier the comparison among results characterized by different values of the Reynolds number (see Fig. 4).

Before the sudden blockage, the velocity profile in the channel is of Poiseuille type and is described by,

$$u_1 = 6\left(x_2 - x_2^2\right), \qquad u_2 = 0. \tag{2}$$

As explained by Weinbaum and Parker [4], at a sufficient distance from the valve, just after the passage of the pressure wave produced by the sudden blockage, the velocity profile is given by (2) minus its average value in the channel width. Then, the initial basic flow can be written as,

$$u_1 = 6\left(x_2 - x_2^2\right) - 1, \qquad u_2 = 0. \tag{3}$$

It can be noted that the velocity profile given by Eq. (3) is characterized by a zero net flow rate and results in a slip velocity at the walls. The subsequent development of the velocity profile (3), with or without 2-D perturbations, is described by the Navier–Stokes and continuity equations which in dimensionless form read,

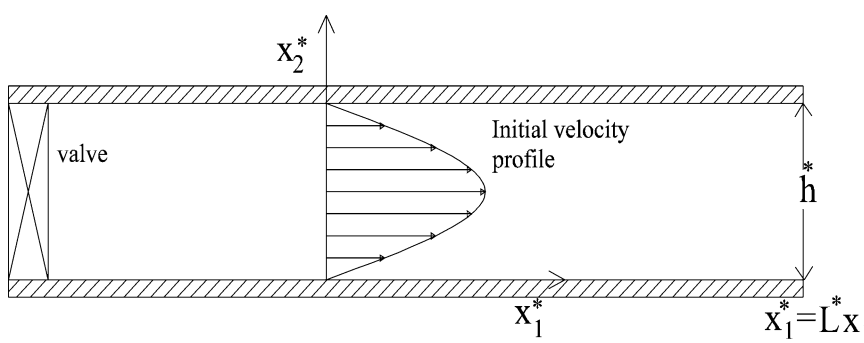

Fig. 1. Sketch of the problem.

$$\frac{\partial u_j}{\partial t} + \frac{\partial u_j u_l}{\partial x_l} = -\frac{\partial p}{\partial x_j} + \delta_{1,j} f + \frac{1}{Re}\frac{\partial^2 u_j}{\partial x_l \partial x_l}, \tag{4}$$

$$\frac{\partial u_l}{\partial x_l} = 0, \tag{5}$$

where j and l take the values (1, 2) to denote the streamwise and cross-stream direction respectively; f is a spatial constant pressure gradient added to the equations in order to get zero flow rate and $\delta_{1,j}$ is the Kronecker delta. The equation that links f to the hydrodynamic variables will be derived in the following.

The governing equations are solved numerically in a rectangular domain of size L_{x_1} and L_{x_2} in the streamwise and cross-stream directions respectively. As the size of the computational domain in the cross-stream direction is equal to the dimensionless channel width h, it follows that $L_{x_2} = h = 1$.

The adopted numerical procedure makes use of spectral methods and finite-difference approximations. At the top and bottom walls the no-slip condition is forced,

$$(u_1, u_2) = 0 \quad \text{at } x_2 = 0 \text{ and } x_2 = 1, \tag{6}$$

while periodic boundary conditions are used in the x_1 direction. To compute streamwise spatial derivatives, all the variables are expanded using truncated Fourier series in the x_1 direction,

$$\big(u_1(t, x_1, x_2), u_2(t, x_1, x_2), p(t, x_1, x_2)\big) = \sum_{n=-N}^{n=N} \big(\hat{u}_{1,n}(t, x_2), \hat{u}_{2,n}(t, x_2), \hat{p}_n(t, x_2)\big)\, \mathrm{e}^{\mathrm{i}n\alpha x_1}, \tag{7}$$

where $\hat{u}_{j,n}$ and $\hat{p}_n$ are the harmonic components of the velocity and of the pressure respectively, N is the number of harmonic components, i is the imaginary unit and $\alpha = 2\pi/L_{x_1}$. Cross-stream spatial derivatives are approximated by centred second order finite-differences. In particular, in the x_2 direction a staggered grid with N_2 grid-points is employed here. The velocity component u_1 and the pressure p are defined at the center of each spatial step Δx_2, while the velocity component u_2 is defined at the end points of the same spatial step. Moreover, in the x_2 direction a nonuniform grid is used in order to cluster the gridpoints in the vicinity of the walls where strong gradients are expected to exist. The clustering is obtained by the following stretching,

$$x_2 = L_{x_2}\frac{\tanh(s) + \tanh[s(2\xi - 1)]}{2\tanh(s)}, \tag{8}$$

where ξ is a dummy variable varying from zero to 1 and s is a stretching parameter. By choosing an uniform grid spacing along ξ, the grid spacing along x_2 is finer close to the walls and coarser close to the channel centerline. The increasing of the value of s results in a more clustering of the grid points close to the walls. An important issue when using nonuniform grids is the spatial order of accuracy of the numerical discretization [9]. The accuracy of the differential operators discretized by the present finite-difference method is of the second order on an equispaced grid. When using a nonuniform grid the accuracy could drop to first order if the grid spacing does not vary smoothly. As the transformation (8) is a continuous function with all its derivatives, we expect that in the present case the second order of accuracy is retained. In all the simulations presented in the following s has been fixed equal to 2.

To evaluate the pressure gradient f which forces zero flow rate in the channel, we take the integral in the computational domain of the Navier–Stokes equation in the streamwise direction. By introducing the boundary conditions, the result of the integration is the following,

$$f = \frac{\partial q}{\partial t} - \frac{1}{Re\, L_{x_1}}\int_{\partial D} \frac{\partial u_1}{\partial n}\, \mathrm{d}\ell, \tag{9}$$

where q is the flow rate in the channel section given by $\int_0^1 u_1\, \mathrm{d}x_2$, ∂D is the no-slip boundary, $\partial/\partial n$ is the derivative in the direction of the unit vector n normal to the boundary and ℓ is the abscissa along ∂D. Finally, considering that the flow rate is zero at all times, (9) becomes,

$$f = -\frac{1}{Re\, L_{x_1}}\int_{\partial D} \frac{\partial u_1}{\partial n}\, \mathrm{d}\ell. \tag{10}$$

This result shows that, in order to force a zero flow rate, the pressure gradient f must balance the viscous stresses at the no-slip walls.

The time advancement of the governing equations employs a fractional step method extensively described by Kim and Moin [10] and Rai and Moin [11]. The convective terms are evaluated explicitly by means of a three-step Runge–Kutta scheme

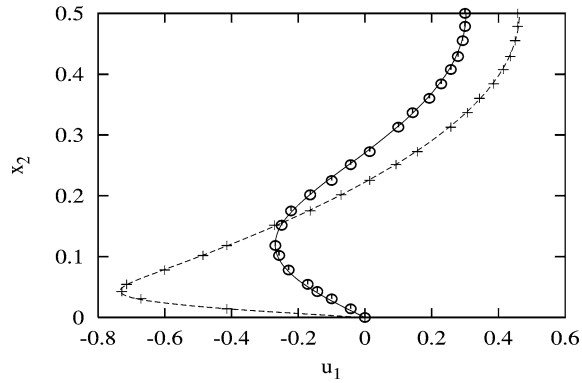

Fig. 2. Comparison between the velocity profiles obtained by Weinbaum and Parker [4] and the velocity profiles obtained by the present approach; markers: Weinbaum and Parker [4]; curves with lines: present results; $+\ t_d = 0.001$; $\circ\ t_d = 0.023$.

[11], while the viscous terms are evaluated implicitly by the Crank–Nicholson scheme. Since the present Runge–Kutta scheme is of the third-order and the Crank–Nicholson scheme is of the second order, the overall accuracy of the method is of the second order in time. The advantage of the Runge–Kutta scheme over one-step schemes lies mainly on its higher stability.

To check the accuracy of the numerical procedure and the reliability of the numerical code, the flow generated by an oscillating pressure gradient has been simulated. In this case two Stokes boundary layers develop close to the walls and the numerical results show a good agreement with the analytical solution. Since the flow in the Stokes boundary layer is determined only by viscous terms, a second test has been performed in order to ascertain the reliability of the numerical code under more general conditions. In this second test the impinging of a Lamb dipole on a wall has been simulated. A fairly good agreement is found between present results and those of Orlandi [12], describing the time development of the vorticity field for $Re = 800$.

To compute the velocity profiles of the basic flow, the system (4), (5) is solved without 2-D perturbations and using Eq. (3) as initial condition. Fig. 2 shows the comparison between two velocity profiles of the basic flow computed by the present approach and those obtained by Weinbaum and Parker [4]. Present results have been obtained using $N_2 = 150$ and a time step $\Delta t = 0.005$. Practically coincident results are obtained by using $N_2 = 75$ and larger time steps.

3. The stability of the basic flow

In this section, the stability of the decaying basic flow is investigated by computing the time development of 2-D velocity perturbations of small amplitude. The aim is to check the reliability of the quasi-steady approach when it is used to study the stability of the present basic flow. As shown by Hall and Parker [8], the growth rate computed by the quasi-steady approach differs from the actual one by an amount of the order of Re^{-1}. Then, as the present basic flow is unstable for quite low values of the Reynolds number, we expect some influence of the unsteadiness of the basic flow on the marginal stability conditions.

By performing a normal mode analysis in the x_1 direction, we consider perturbations superimposed on the basic flow in the form,

$$\big(u_1'(t_d, x_1, x_2), u_2'(t_d, x_1, x_2)\big) = \varepsilon\big(\hat{u}_{1,1}'(t_d, x_2)\,\mathrm{e}^{\mathrm{i}\alpha x_1} + c.c., \hat{u}_{2,1}'(t_d, x_2)\,\mathrm{e}^{\mathrm{i}\alpha x_1} + c.c.\big), \tag{11}$$

where ε is a small parameter and $c.c.$ denotes the complex conjugate of a complex number. To investigate the stability of the basic flow, we solve numerically the initial value problem posed by the Navier–Stokes and continuity equations for given initial form of the function $\hat{u}_{1,1}'$ and $\hat{u}_{2,1}'$ and for fixed values of the parameters L_{x_1} and Re. To evaluate the growth of the perturbation, we compute the function $g(t_d)$ defined as,

$$g(t_d) = \frac{I(t_d)}{I_0}, \quad I(t_d) = \sqrt{\frac{\int_0^{L_{x_1}} \int_0^{L_{x_2}} (u_1'^2 + u_2'^2)\,\mathrm{d}x_1\,\mathrm{d}x_2}{L_{x_1} L_{x_2}}}, \tag{12}$$

where I_0 is the initial value of $I(t_d)$.

The flow is said to be unstable if at some time during the simulation $g(t_d)$ tends to grow and it is said to be stable if $g(t_d)$ is monotonically decreasing. In the plane (L_{x_1}, Re), the boundary between these two behaviours of the function $g(t_d)$ defines the neutral stability curve.

A possible choice of $\hat{u}_{1,1}'$ and $\hat{u}_{2,1}'$ is to consider random functions of x_2. Unfortunately, since we are investigating the stability of a basic flow which decays in time, this procedure would give rise to some complications. Indeed, a random

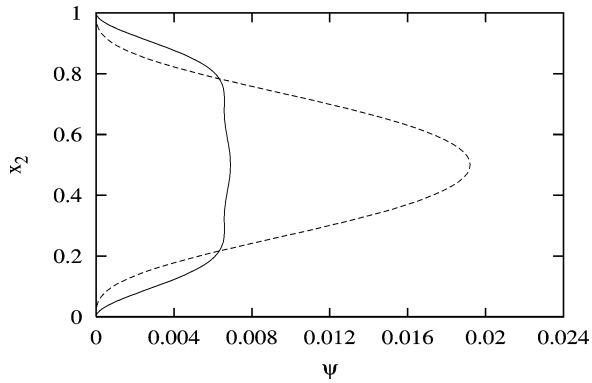

Fig. 3. Most unstable eigenfunction for $L_{x_1} = 1.508$ and $Re = 199.6$; continuous line: real part; dotted line: imaginary part.

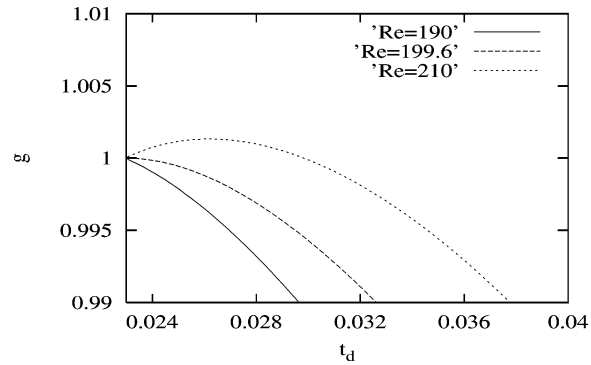

Fig. 4. Time development of the function $g(t_d)$ for perturbations of small amplitude. $L_{x_1} = 1.508$.

perturbation can be thought as the sum of many components with respect to a certain orthogonal basis. Generally, for unstable conditions, only a few of these components grow, while all the others decay. Moreover, since the basic flow tends to decay on a relatively short time, the amplification of the unstable components takes place only during a limited time interval. Hence, the decay of the stable components can obscure the growth of the unstable ones. This problem is particularly severe when values of (L_{x_1},*Re*) close to the neutral stability curve are considered. An attempt to circumvent this problem was made by choosing as initial values of $\hat{u}'_{1,1}$ and of $\hat{u}'_{2,1}$ the most unstable eigenmode determined by Hall and Parker [8] who found that the most unstable velocity profile is generated at $t_d = 0.023$ for any value of the Reynolds number.

Since Hall and Parker [8] did not provide numerical values for $(\hat{u}'_{1,1}, \hat{u}'_{2,1})$, it has been necessary to perform again their linear stability analysis based on a quasi-steady approach. Following Hall and Parker [8], the basic flow is perturbed by disturbances in the form,

$$\psi(t_d, x_1, x_2) = \varepsilon \hat{\psi}(x_2)\, \mathrm{e}^{\mathrm{i}\alpha(x_1 - c t_d)} + c.c., \tag{13}$$

where ψ is the stream function describing the flow perturbation and c is a complex number. Substituting (13) in the Navier–Stokes equations, neglecting terms of order ε^2 and using a quasi-steady approach, the well known Orr–Sommerfeld equation is obtained. The eigenvalue problem posed by the Orr–Sommerfeld equation has been solved by a shooting method and a fourth-order Runge–Kutta numerical scheme. The present neutral stability curve computed at $t_d = 0.023$ is practically coincident with that of Hall and Parker [8] with differences of the order of 1%. These small discrepancies could be due to the different numerical procedure used by Hall and Parker [8] with respect to the present one. The critical value of the Reynolds number turns out to be 199.6 and the critical wavelength L_{x_1} is 1.508 ($\alpha = 4.166$). In Fig. 3 the real and the imaginary parts of the most unstable eigenfunction computed for $L_{x_1} = 1.508$ and $Re = 199.6$ are plotted.

To investigate the stability of the flow when the assumption of a slowly varying basic flow is removed, first the values of L_{x_1} and *Re* are chosen, then the basic flow is perturbed at $t_d = 0.023$ (i.e., when the most unstable velocity profile is generated) by introducing a disturbance of the form (11) and finally the development of the perturbation is simulated using the numerical code, thus allowing the basic flow to develop in time. In these simulations only one harmonic component has been introduced to describe the flow in the streamwise direction because of the assumed linearity, while 150 grid points have been used in the x_2 direction. The value of the parameter ε is fixed at 10^{-3}. It has been ascertained that this value of ε is small enough to keep the evolution of the perturbation linear.

In Fig. 4 $g(t_d)$ is plotted versus t_d for *Re* equal to 190, 199.6 and 210 with $L_{x_1} = 1.508$. We note that for $Re = 190$ the perturbation tends immediately to decay. For $Re = 199.6$, at the beginning the flow appears in a neutral state and then tends to decay. Finally, for $Re = 210$ a short time interval is present during which $g(t_d)$ grows and the flow can be defined unstable in the sense described above. According to the theoretical results of Hall and Parker [8], it has been observed that when values of L_{x_1} and *Re* are fixed such that the point (L_{x_1}, *Re*) lies on the neutral stability curve they predicted, the perturbation at the beginning neither grows nor decays. Then, for larger times a decay of the disturbance is observed because, as theoretically predicted by Hall and Parker [8], for $t_d > 0.023$ the flow turns out to be stable.

A second set of runs has been made where the values of L_{x_1} and *Re* have been set equal to 1.508 and 199.6 respectively and the most unstable mode computed at $t_d = 0.023$ have been added to the basic flow either at $t_d > 0.023$ or at $t_d < 0.023$. When the basic flow is perturbed at $t_d > 0.023$, according to Hall and Parker [8], a decay of the function $g(t_d)$ is observed. On the contrary, when the basic flow is perturbed at $t_d < 0.023$ a time interval exists during which the function $g(t_d)$ grows and the flow can be defined unstable. In Fig. 5 the maximum value $g_{\max}$ attained by the function $g(t_d)$ is plotted versus the

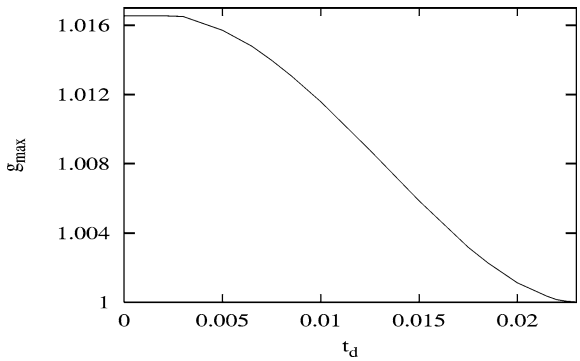

Fig. 5. Maximum values attained by the function g versus the time t_d at which the basic flow is perturbed for $L_{x_1} = 1.508$ and $Re = 199.6$.

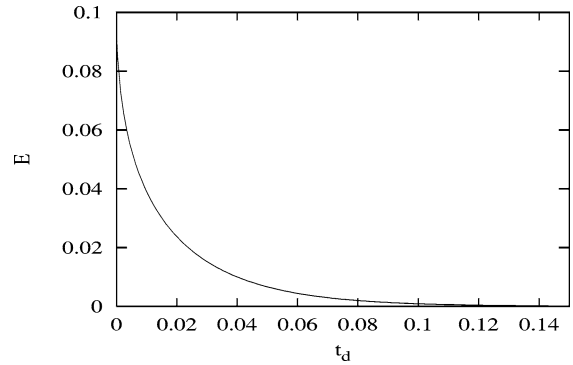

Fig. 6. Time development of the kinetic energy of the basic flow for $Re = 199.6$.

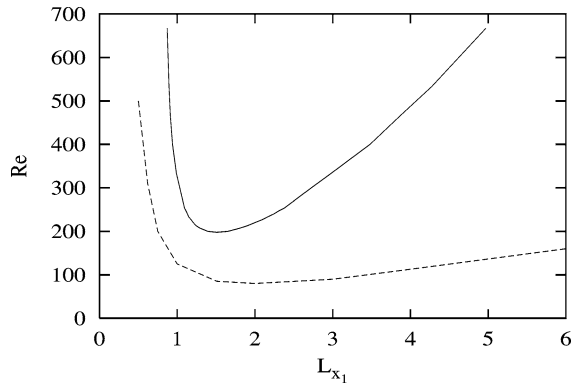

Fig. 7. Neutral stability curves; continuous line: Hall and Parker [8], dashed line: present results.

time t_d at which the basic flow is perturbed. It can be noted that $g_{\max}$ is a decreasing function of t_d and assumes the value 1 at $t_d = 0.023$. On the grounds of these results it can be stated that, in the range $0 \leqslant t_d < 0.023$, the quasi-steady approach does not exactly reproduce the actual marginal stability conditions of the flow. Indeed, for $Re = 199.6$ the quasi-steady approach predicts stable conditions for all times except for $t_d = 0.023$. The larger deviation of present results from the ones predicted by the quasi-steady approach, that can be observed when the flow is perturbed at $t_d = 0$, could be due to the occurrence that immediately after the sudden blockage the decay rate of the basic flow is large, thus making the hypothesis of slowly varying basic flow not entirely fulfilled. Indeed, in Fig. 6, where the kinetic energy E of the basic flow is plotted versus the time t_d, it can be seen that the decay rate is large at $t_d = 0$ and then it tends asymptotically to zero as t_d tends to infinity.

Stimulated by these findings a last set of runs was performed for several values of L_{x_1} and Re, with the basic flow perturbed at $t_d = 0$ by the most unstable mode computed at $t_d = 0.023$. In Fig. 7 the neutral stability curve computed by the present procedure is compared with the one of Hall and Parker [8]. It clearly appears that for every perturbation wavelength the basic flow is more unstable than predicted by the quasi-steady approach. For low values of L_{x_1} the two neutral stability curves are not very far from each other. The most important differences are observed for large values of L_{x_1}.

Before closing this section, it should be put in evidence that for values of Reynolds numbers lying below the neutral stability curve of Hall and Parker [8], the maximum amplification of the disturbances is small (see Fig. 5). Then, the quasi-steady approach appears to be appropriate for a first evaluation of the stability of the present basic flow.

4. The structure of the unstable flow field

Up to now we have considered the basic flow subject to disturbances of small amplitude such that their development can be evaluated by means of a linear approach. In this section the velocity field is studied when the basic flow is perturbed with disturbances of significant amplitude such that nonlinear effects become important. In this case the number of harmonic components in (7) must be fixed in such a way that a reliable description of the velocity field is obtained.

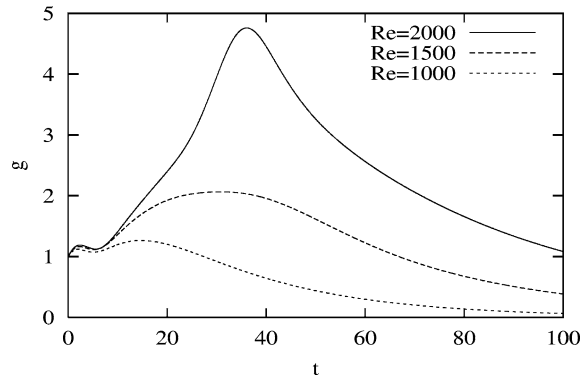

Fig. 8. Time development of the function $g(t)$ for perturbations of significant amplitude. $L_{x_1} = 6$.

In the following, results of simulations with the basic flow perturbed at $t = 0$ either by a regular perturbation or by a random perturbation are presented. The regular perturbation is of the form (11), determined by using the most unstable eigenmode as predicted by Hall and Parker [8] and fixing $\varepsilon = 0.2$. Thus, for the case of the regular perturbation, only the first harmonic component is initially introduced and the remaining ones are generated because of nonlinear effects. As regards the random perturbation, first random values for u_2' are generated and then u_1' is computed from the continuity equation. To generate the random function u_2', a double expansion is introduced where Fourier series are used in the x_1 direction while Chebyshev series are used in the x_2 direction,

$$u_2'(x_1, x_2) = \sum_{n=-N}^{n=N} \sum_{m=0}^{N_c} A_{n,m}\, \mathrm{e}^{\mathrm{i}n\alpha x_1} T_m(2x_2 - 1), \tag{14}$$

where $T_m(2x_2 - 1)$ is the Chebyshev polynomial of order m. For each integer n, $Nc - 4$ complex components $A_{n,m}$ have been generated randomly with phases and modules uniformly distributed in the intervals $(0, 2\pi)$ and $(0, Z)$ respectively, by means of a library Fortran routine. The remaining four $A_{n,m}$ components have been computed in such a way that the following boundary conditions are forced,

$$u_2' = \frac{\partial u_2'}{\partial x_2} = 0 \quad \text{at } x_2 = 0, 1. \tag{15}$$

The use of the Chebyshev polynomials allows to force (15) easily, indeed the remaining four components have been computed by solving the following linear system,

$$\sum_{m=0}^{Nc} A_{n,m} = 0, \qquad \sum_{m=0}^{Nc} (-1)^m A_{n,m} = 0, \qquad \sum_{m=0}^{Nc} m^2 A_{n,m} = 0, \qquad \sum_{m=0}^{Nc} (-1)^m m^2 A_{n,m} = 0. \tag{16}$$

The positive value Z has been fixed in such a way that both the maximum absolute value of u_2' and of u_1' do not exceed the 3% of the maximum absolute value of the basic flow.

First, let us describe the results obtained by introducing the regular disturbance. In Fig. 8 the time development of $g(t)$ is plotted for $L_{x_1} = 6$ and different values of the Reynolds number. For $Re = 1000$ the flow shows only an initial weak instability even though the value of the Reynolds number is significantly larger than the critical one. When $Re = 1500$ the flow appears to be significantly perturbed by the growth of the initial perturbation. For the largest value of Re ($Re = 2000$), $g(t)$ is characterized by a well marked initial exponential growth of the perturbation. The growth is stopped both by the generation of higher harmonic components which allow the viscosity to operate more effectively and by the decay of the basic flow, i.e., by a decrease of the energy transfer from the basic flow. These simulations have been performed using $N = 63$ for $Re = 2000$ and $Re = 1500$, $N = 31$ for $Re = 1000$, while the number of gridpoints N_2 in the cross-stream direction have been fixed equal to 150 in all the cases. It has been ascertained that the number of grid points is sufficient to have a fair description of the flow. The dynamics of vortices observed in the present simulations is qualitatively the same as that observed in the experimental visualizations described by Weinbaum and Parker [4] and Das and Arakeri [5] (see the introduction). However, it should be stressed that in most cases the turbulence observed in the final stage of the experimental visualizations is 3-D, therefore it cannot be claimed that present 2-D flow simulations provide a realistic description of the actual flow field. Nevertheless, at the initial stage the perturbation behaves as 2-D and reliable results are obtained by the present numerical simulations. One of the reasons for studying 2-D perturbations is related to the many examples of bounded flows, such as pipe flow [13] and Stokes boundary

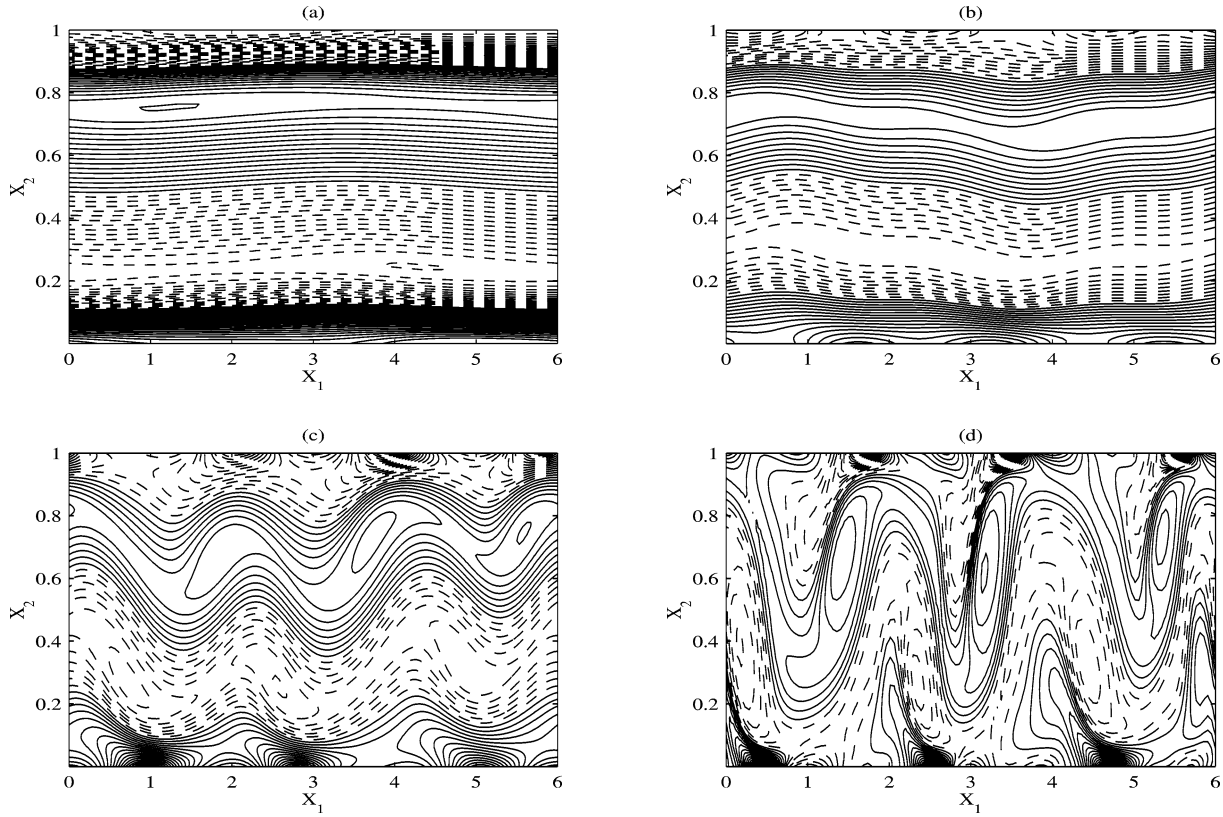

Fig. 9. Time development of the vorticity for $L_{x_1} = 6$ and $Re = 2000$; (a) $t = 10.05$; (b) $t = 20.10$; (c) $t = 30.15$; (d) $t = 40.20$. $\Delta\omega = 0.18$ (dashed lines: negative vorticity, continuous lines: positive vorticity).

layer [2], for which it is known that the transition to a 3-D flow takes place because of the instability of two-dimensional waves of finite amplitude with respect to infinitesimal spanwise disturbances.

Fig. 9 shows the vorticity contour plot at different times during the perturbation development for $Re = 2000$. At $t = 0$ two very thin layers with high vorticity are present near the two walls. At $t = 10.05$ these vortex layers have diffused to some extent as it can be seen in Fig. 9(a), where the periodic perturbation superimposed on the basic flow is also detectable. During the first stage of the growth of the perturbation, the mechanism of instability can be understood using the results of the linear stability theory by Hall and Parker [8]. The presence of an inflexion point in the velocity profile makes the basic flow inviscidly unstable. In the flow under consideration viscous effects are acting as well, but inviscid instability is much more vigorous. Different authors explained how inviscid instability acts [14]. Near the lower wall a vortex layer of negative vorticity is present which contains the inflexion point in the velocity profile at $x_2 = \bar{x}_2$. When a perturbation is superimposed on the basic flow the vortex layer becomes wavy in the streamwise direction. For small amplitude perturbations, the linearized vorticity equation shows that the vorticity transport close to the inflection point is mainly due to the basic flow. In a reference system travelling with the velocity of the basic flow at the inflexion point, for $x_2 > \bar{x}_2$ the basic flow is positive and for $x_2 < \bar{x}_2$ it is negative, then crests and troughs of the perturbation move in opposite directions. This causes the steepening of the vortex layer and the roll-up of the vorticity because of the self-induced velocity. At later stages nonlinear effects are not negligible and the further development of the instability cannot be described in the framework of the linear stability theory. Furthermore, the above description could be exhaustive only for free shear flows. In the present case, close to the wall a layer of positive vorticity, in the following referred as wall layer, is also present (Fig. 9 (a) and (b)). During the growth of the perturbation, the wavinesses of the vortex layer and that of the wall layer increase until coupling of vortices of opposite signs occurs. Coupling gives rise to ejections of positive vorticity towards the channel centerline and the entrainment of negative vorticity in the region near the wall (Fig. 9 (c) and (d)). The opposite happens near the upper wall. Then a periodic pattern emerges that appears in agreement with the experimental observations [4,5]. The ejection of vorticity from a boundary into the flow has also been observed in simulations of decaying 2-D turbulence in containers with no-slip boundaries [15,16].

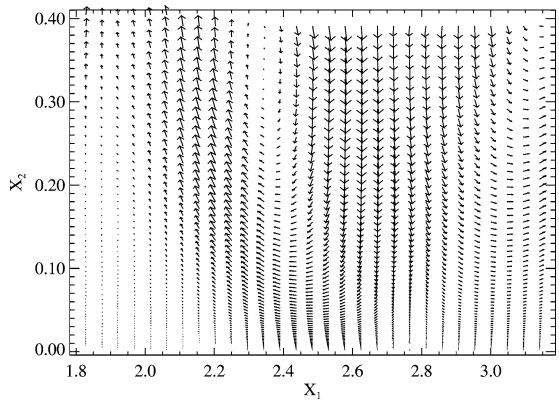

Fig. 10. Velocity field at $t = 40.20$ for $L_{x_1} = 6$ and $Re = 2000$.

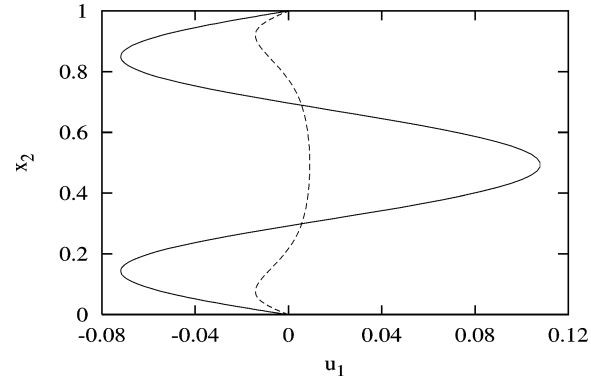

Fig. 11. Basic flows for $Re = 2000$ at $t = 40.20$; continuous line: unperturbed basic flow; dashed line: perturbed basic flow.

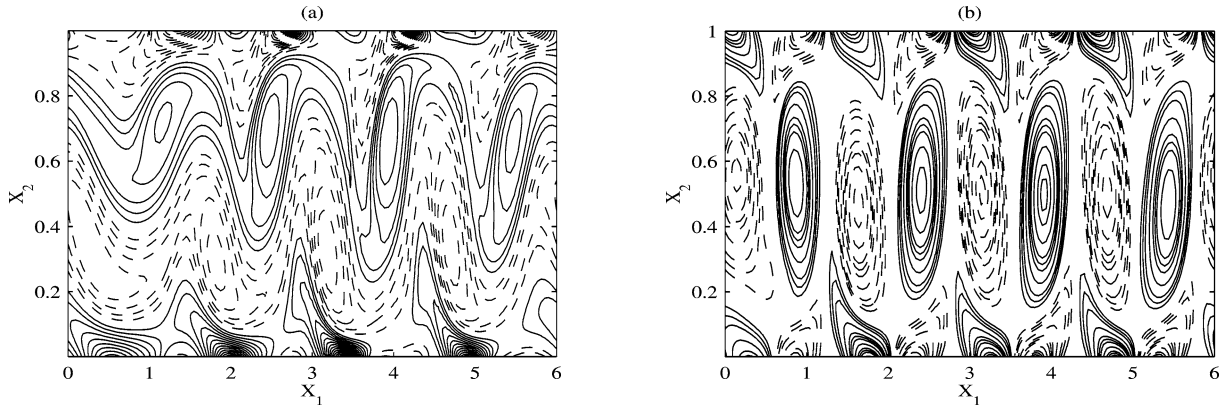

Fig. 12. Vorticity field for $L_{x_1} = 6$ and $Re = 2000$; (a) $t = 40.20$, $\Delta\omega = 0.18$, (b) $t = 70.35$, $\Delta\omega = 0.06$ (dashed lines: negative vorticity, continuous lines: positive vorticity); the basic flow is perturbed by a random disturbance.

The turbulence observed during the final stage of the experiments [4,5] is due to a three-dimensional instability of the two-dimensional vortices. It can be expected that the ejection regions are characterized by a significant upward velocity. Indeed, in Fig. 10, where the velocity field is plotted for $1.8 \leqslant x_1 \leqslant 3.2$ and $0 \leqslant x_2 \leqslant 0.4$, it clearly appears that the ejection of positive vorticity near the abscissa $x_1 = 2$ is associated with a strong upward velocity. Because of continuity constraints, significant downward velocity is present as well.

The above structure of the flow field implies a strong mixing between fluid near to the channel centerline and fluid near to the walls which occurs at expenses of the energy of the basic flow. As a consequence the basic flow undergoes a fast decay as it can be seen in Fig. 11, where the basic flow (i.e., the harmonic component $\hat{u}_{1,0}$) is plotted at $t = 40.20$ along with the basic flow obtained in the unperturbed case. It can be noted that the velocity profile of the basic flow is symmetric with respect to the channel centerline. This result can be easily explained considering that the stream function of the most unstable mode used to perturb the flow is an even function with respect to the channel centerline. This consideration also explains why a π phase difference between the top and bottom vortices is present in Fig. 9. However, a tendency to develop a π phase difference is observed even though the basic flow is perturbed by a random disturbance as shown in Fig. 12(a), where the vorticity contour plot of a simulation at $Re = 2000$, performed by using $N = 63$, $N_2 = 150$ and $N_c = 73$, is reported at about the time at which the energy of the perturbation reaches the maximum value. Therefore, the preferential mode of instability is even, as predicted by the linear stability theory, also for disturbances of not small amplitude. These observations were first made by Das and Arakeri [5] on the basis of their channel flow visualizations. As a π phase difference is also observed in pipe flow, the above mentioned authors argued that in this case the most unstable mode is an helical mode.

In Fig. 12(b) the vorticity field after the flow has evolved for further 30.15 time units with respect to Fig. 12(a) is shown. It can be observed that along the streamwise direction the flow is organized into a sequence of vortices with alternating signs. These vortices, which are already present in Fig. 12(a), arise directly from the inviscid instability at the inflexion points of the basic flow previous discussed. The fact that vortices with the same sign remain separated, prevents the formation of larger

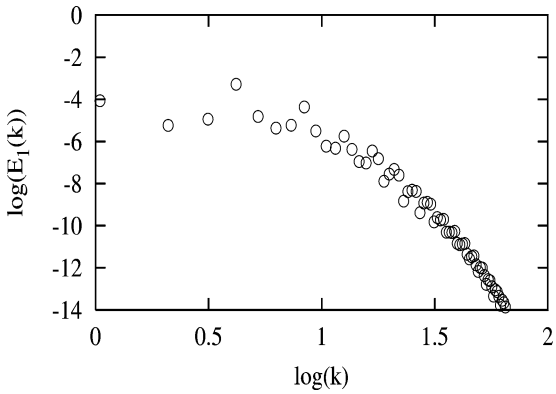

Fig. 13. Spectrum $E_1(k)$ at $t = 40.20$ for $L_{x_1} = 6$ and $Re = 2000$; the basic flow is perturbed by a random disturbance.

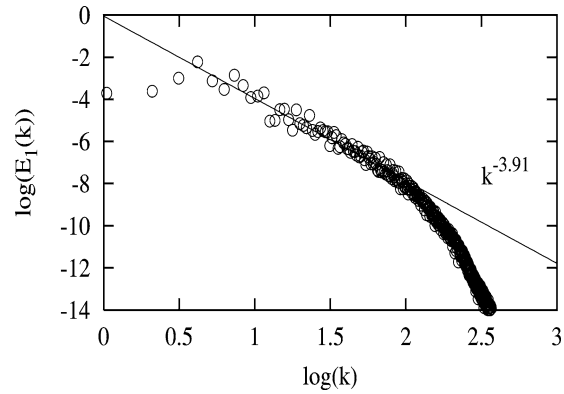

Fig. 14. Spectrum $E_1(k)$ at $t = 40.20$ for $L_{x_1} = 6$ and $Re = 10000$; the basic flow is perturbed by a random disturbance.

vortices generated by the merging process. It has been observed that the structure of the vorticity field shown in Fig. 12(b) remains qualitatively unchanged during all the decay process.

Further insight into the structure of the flow field can be gained considering the spatial spectrum of the flow variables. The harmonic components in the streamwise direction are computed during the time advancement of the governing equations. Hence, the one dimensional energy spectrum $E_j(k_n, t)$ can be easily obtained,

$$E_j(k_n, t) = \frac{1}{L_{x_2}} \int_0^{L_{x_2}} \left|\hat{u}_{j,n}(t, x_2)\right|^2 \mathrm{d}x_2, \tag{17}$$

where $k_n = n2\pi/L_{x_1}$. An analogous approach have been used by Lesieur et al. [17] in a different context.

In the case shown in Fig. 9 only the component of the spectrum characterized by the wavenumber k_1 is introduced at the beginning of the simulation. At $t = 30$ the peak in the spectrum is still on k_1, but at $t = 40.20$ the peak is on k_3 and remains there during all the decay process. Different results are obtained if a random disturbance is introduced to perturb the basic flow. In this case the peak wavenumber is on k_4 for both the velocity components. It is put in evidence that k_4 is the most amplified wavenumber according to the linear stability theory. The localization of the peak wavenumber on k_4 is also congruent with the presence of 4 ejections of vorticity near the walls that are clearly visible in Fig. 12(a). Analogous results are obtained when the streamwise length of the computational box L_{x_1} is doubled.

In Fig. 13 the energy spectrum of the u_1 velocity component is plotted at $t = 40.20$. It can be observed that a power law range can be hardly appreciated. A power law spectrum does not emerge because the flow is not characterized by a well developed turbulent state. In order to reach a turbulent state one could try to evolve the flow further in time. However, it should be taken into account that the two-dimensional perturbations extract their energy from the basic flow which tends to decay (see Fig. 6). For this reason, to evolve the flow further in time does not lead to a turbulent state. Indeed, at $t = 70.35$ the vorticity field is characterized by a regular pattern (Fig. 12(b)) which shows that the flow is evolving towards a viscous dominated state. To make clear the features of the spectrum one must obtain more separation between the scale of the vortices generated by the inviscid instability and the scale at which enstrophy dissipation occurs. Generally, a larger separation between these scales can be achieved by increasing the value of the Reynolds number.

In Fig. 14 the energy spectrum of the u_1 velocity component at $t = 40.20$ for a computation at $Re = 10000$ involving 399 harmonics components in the streamwise direction and 350 grid points in the cross-stream direction is reported. In this simulation the random disturbance has been obtained by assuming $N_c = 153$. It can be observed that a power law range has now emerged. Fitting a straight line to the spectrum in the range $\log(k) = (0.62, 1.90)$ by using least squares, it has been estimated that the exponent of the power law assumes the value -3.91. The energy spectrum of the u_2 velocity component and that of the total energy also exhibits a power law range but with exponents equal to -3.47 and -3.59 respectively.

Spectra of two-dimensional flows displaying slopes ranging from -3 to -4 have been found in different contexts. Lesieur et al. [17] found a k^{-4} spectrum after the first vortex pairing in a temporal mixing layer. The above mentioned authors also found that after the second vortex pairing the spectrum follows an intermediate law between k^{-3} and k^{-4}. Nielsen et al. [18] obtained a k^{-4} inertial range spectrum by numerical simulating the merging of two identical vortices. In two-dimensional isotropic turbulence, where according to the classical theory of the enstrophy cascade a k^{-3} spectrum should be present [19,20], laws

close to k^{-4} have been obtained as well [21,22]. In general, the spectrum of a two-dimensional turbulence can range from k^{-3} to k^{-6} and the departure from k^{-3} is usually associated with the presence of long-lived coherent vortices [22].

It can be observed that the spectrum in Fig. 14 does not show the $k^{-5/3}$ power law range due to the inverse energy cascade [19,20], which is also absent in the results of Lesieur et al. [17]. However, the inverse energy cascade is also not clearly observed in decaying 2-D turbulence with double periodic boundary conditions [15].

An explanation of the development of a k^{-4} energy spectrum in isotropic turbulence has been given by Saffman [23] considering the presence of vorticity discontinuities. The present $k^{-3.91}$ energy spectrum of the u_1 velocity component is quite close to k^{-4} but the $k^{-3.59}$ spectrum of the total energy is more close to $k^{-11/3}$ predicted by Gilbert [24] for spiral structures.

Recent important developments have put in evidence that the no-slip boundaries exert a peculiar role on the evolution of a 2-D decaying turbulence [16,25]. It has been observed that when the spectra are computed close to a no-slip boundary, during the initial decay stage, they show a $k^{-5/3}$ spectrum range up to the smallest resolved scales. When the spectra are computed at larger distance from the no-slip boundaries, the $k^{-5/3}$ spectrum tends to disappear and to be replaced by a steeper one. As explained in [16,25], the appearance of a $k^{-5/3}$ spectrum is due to the vortex wall interaction which generates small scale vorticity characterized by a certain wavenumber k_i. As the present flow interacts with a no-slip boundary, it is tempting to check if the spectra computed close to the boundary show also a $k^{-5/3}$ power law. Therefore, we have computed the spectra as follows,

$$E_j(k_n, x_2, t) = \frac{1}{2}\left[\left|\hat{u}_{j,n}(t, x_2)\right|^2 + \left|\hat{u}_{j,n}(t, L_{x_2} - x_2)\right|^2\right]. \tag{18}$$

Several spectra have been computed varying x_2 in the range $[0, 0.5]$ and t in the range $(0, 100)$ for the simulation at $Re = 10000$, but a $k^{-5/3}$ spectrum range could not be clearly appreciated in no one case. A possible explanation of this result is that the present value of the Reynolds number is not high enough. Indeed, as discussed in [16], the higher the Reynolds number the more evident appears the $k^{-5/3}$ spectrum. However, simulations at much higher values of the Reynolds number are not possible due to the limited power of the available computers.

Generally, when $Re = 10000$, as in the last presented simulation, unless particular experimental precautions are taken, the actual flow is characterized by a three-dimensional turbulent state. In these conditions it cannot be claimed that the numerical results reproduce the actual flow. It seems reasonable that even in the turbulent case the average velocity profile develops an inflexion point and undergoes an inviscid instability with the generation of quasi 2-D coherent vortices. However, in this case the quantitative prediction of the phenomenon requires the interaction between the background turbulent field and the 2-D vortex structures to be simulated.

5. Conclusions

In this paper the instability mechanism of a laminar channel flow subject to a sudden blockage has been enlightened by numerical solutions of the Navier–Stokes and continuity equations. First, the velocity profile of the decaying flow, as obtained by Weinbaum and Parker [4], has been recovered by the present approach. The analysis of Hall and Parker [8], who investigated the linear stability of the flow using a quasi-steady approach, has been extended by taking into account the unsteadiness of the basic flow. The results show that the flow is more unstable when the unsteadiness of the basic flow is taken into account. However, the quasi-steady approach appears to be appropriate for a first evaluation of the stability of the basic flow.

Simulations performed in the nonlinear regime have reproduced a vorticity field that is consistent with the experimental observations described by Weinbaum and Parker [4] and Das and Arakeri [5]. During the development of the instability the waviness of a vortex layer, far from the wall, grows because of an inviscid instability driven by the presence of an inflexion point. At the same time the vortex layer close to the wall, characterized by vorticity of opposite sign, increases its waviness as well. In the final stage of the growth of the instability vorticity rolls up generating coherent vortices of opposite sign. Near the lower wall this causes the ejection of positive vorticity towards the centerline of the channel and the entrainment of negative vorticity in the region near the wall.

It has been shown that when the value of the Reynolds number is high enough, a wavenumber range exists in which the spatial longitudinal energy spectrum displays a power law intermediate between k^{-3} and k^{-4}. This result is due to the appearance of coherent structures and is the same as that obtained by other authors for two-dimensional flows.

In the water hammer in pipe flows, pressure waves travels many times back and forth along the pipe before the basic flow becomes to rest and originate an oscillatory flow the stability of which may substantially differ from that presently investigated. Therefore, we plan to extend the present study to this unsteady basic flow to see how the oscillatory character of the basic flow modifies present results.

Acknowledgements

The financial support of the Italian Ministry of Education, University and Research through the National Project on "Influence of vorticity and turbulence in interactions of water bodies with their boundary elements and effects on hydraulic design" is gratefully acknowledged. Many tanks are due to Prof. P. Blondeaux and to Prof. G. Pezzinga for helpful comments during the course of this work.

References

[1] R. Akhavan, R.D. Kamm, A.H. Shapiro, An investigation of transition to turbulence in bounded oscillatory Stokes flows. Part 1. Experiments, J. Fluid Mech. 225 (1991) 395–422.
[2] R. Akhavan, R.D. Kamm, A.H. Shapiro, An investigation of transition to turbulence in bounded oscillatory Stokes flows. Part 2. Numerical simulations, J. Fluid Mech. 225 (1991) 423–444.
[3] R.M. Nerem, W.A. Seed, An in vivo study of aortic flow disturbances, Cardiovasc. Res. 6 (1972) 1–14.
[4] S. Weinbaum, K.H. Parker, The laminar decay of suddenly blocked channel and pipe flows, J. Fluid Mech. 69 (1975) 729–752.
[5] D. Das, J.H. Arakeri, Transition of unsteady velocity profiles with reverse flow, J. Fluid Mech. 374 (1998) 251–283.
[6] G. Pezzinga, Quasi-2D model for unsteady flow in pipe networks, J. Hydr. Engrg. ASCE 125 (7) (1999) 676–685.
[7] A.E. Vardy, K.L. Hwang, A characteristics model of transient friction in pipes, J. Hydr. Res. 29 (1990) 669–684.
[8] P. Hall, K.H. Parker, The stability of the decaying flow in a suddenly blocked channel, J. Fluid Mech. 75 (1976) 305–314.
[9] J.D. Hoffman, Relationship between the truncation errors of centered finite-difference approximations on uniform and nonuniform meshes, J. Comp. Phys. 46 (1982) 469–474.
[10] J. Kim, P. Moin, Application of a fractional-step method to incompressible Navier–Stokes equation, J. Comp. Phys. 59 (1985) 308–323.
[11] M.M. Rai, P. Moin, Direct simulations of turbulent flow using finite-difference schemes, J. Comp. Phys. 96 (1991) 15–53.
[12] P. Orlandi, Vortex dipole rebound from a wall, Phys. Fluids A 2 (8) (1990) 1429–1436.
[13] S.A. Orszag, A.T. Patera, Secondary instability of wall-bounded shear flows, J. Fluid Mech. 128 (1983) 347–385.
[14] P.G. Drazin, W.H. Reid, Hydrodynamic Stability, Cambridge University Press, 1981.
[15] H.J.H. Clercx, S.R. Maassen, G.J.F. van Heijst, Decaying two-dimensional turbulence in square containers with no-slip or free-sleep boundaries, Phys. Fluids 11 (1999) 611–626.
[16] H.J.H. Clercx, G.J.F. van Heijst, Energy spectra for decaying 2D turbulence in a bounded domain, Phys. Rev. Lett. 85 (2000) 306–309.
[17] M. Lesieur, C. Staquet, P. Le Roy, P. Comte, The mixing layer and its coherence examined from the point of view of two-dimensional turbulence, J. Fluid Mech. 192 (1988) 511–534.
[18] A.H. Nielsen, X. He, J. Juul Rasmussen, T. Bohr, Vortex merging and spectral cascade in two-dimensional flows, Phys. Fluids 8 (1996) 2263–2265.
[19] R.H. Kraichnan, Inertial ranges in two-dimensional turbulence, Phys. Fluids 10 (1967) 1417–1423.
[20] G.K. Batchelor, Computation of the energy spectrum in homogeneous two-dimensional turbulence, Phys. Fluids, Suppl. II 12 (1969) 233–239.
[21] J.R. Herring, J.C. McWilliams, Comparison of direct numerical simulation of two-dimensional turbulence with two-point closure: the effects of intermittency, J. Fluid Mech. 153 (1985) 229–242.
[22] A. Babiano, C. Basdevant, B. Legras, R. Sadourny, Vorticity and passive-scalar dynamics in two-dimensional turbulence, J. Fluid Mech. 183 (1987) 379–397.
[23] P.G. Saffman, On the spectrum and decay of random 2D vorticity distributions at large Reynolds number, Stud. Appl. Math. 50 (1971) 377.
[24] A.D. Gilbert, Spiral structures and spectra in two-dimensional turbulence, J. Fluid Mech. 193, 475–497.
[25] H.J.H. Clercx, A.H. Nielsen, D.J. Torres, E.A. Coutsias, Two-dimensional turbulence in square and circular domain with no-slip walls, Eur. J. Mech. B Fluids 20 (2001) 557–576.